CMS Physics Analysis Summary

Contact: cms-pag-conveners-heavyions@cern.ch 2016/07/30

Transverse momentum balance of b-jet pairs in pp and PbPb collisions at $\sqrt{s_{NN}}$ = 5.02 TeV

The CMS Collaboration

Abstract

The transverse momentum imbalance of pairs of b jets in PbPb and pp collisions at a center-of-mass energy of 5.02 TeV per nucleon pair recorded with the CMS detector at the LHC is reported. A growing mean imbalance is observed with increasing collision centrality, as expected from the jet quenching effect. The data are compared to a measurement with non-identified dijets. A similar level of imbalance is observed within the uncertainties.

1 Introduction

The jet quenching phenomenon is widely believed to be the signature of the parton energy loss process in hot and dense nuclear matter. The first observable used to probe this phenomenonon at the LHC was the transverse momentum (p_{T}) balance of dijet pairs in PbPb collisions [1, 2]. Quenching imparts a net imbalance to dijet pairs, which exceeds that produced by QCD radiation and detector resolution effects, as measured from pp collisions. The cause of this anomalous imbalance is that the quenching varies jet-by-jet, due to variation of both the path-length through the quark-gluon plasma, as well as via fluctuations of the parton energy process itself. By selecting the leading jet in an event, jets that have suffered little quenching are preferentially chosen, whereas the subleading recoil jets tend to sample a larger path-length, and therefore suffer a larger quenching. Quenched jets deposit energy into low p_{T} particles at large angles such that the quenched energy is no longer associated with the reconstructed jet [2, 3]. In this way, the dijet imbalance becomes a particularly sensitive probe of the interaction of hard scattered partons with the quark-gluon plasma.

The dependence of jet quenching on parton mass and flavor remains poorly known. As radiative energy loss is thought to be the dominant mechanism, gluons are expected to lose more energy than quarks, due to their larger Casimir color factor. On the other hand, radiation from massive quarks is expected to be suppressed in the direction of propagation, the so-called dead-cone effect [4], at least for energies not much larger than the quark mass. Jets initiated by b quarks are an excellent observable to test these expectations, given that they are readily identifiable via b-tagging methods. The first steps in this direction were already taken via the measurement of b-jet spectra and corresponding nuclear modification factors in 2.76 TeV PbPb collisions [5]. While no strong dependence of quenching on parton species was evident, the measurement suffers from fairly sizable uncertainties.

In this document, we present the first measurement of p_{T} balance of pairs of b jets (b dijets), which is less sensitive to jet reconstruction and b-tagging systematic uncertainties compared to a measurement of the nuclear modification factor. The b-jet pair measurement has the additional advantage that it preferentially selects jets from b quarks that emerge directly from the primary hard scattering. At next-to-leading order in perturbative QCD, heavy quark production proceeds by three distinct processes, usually denoted by flavor creation (FCR), flavor excitation (FEX) and gluon splitting (GSP), which tend toward different topologies in the final state. The selection of back-to-back pairs preferentially selects primary b jets from the FCR process. In contrast, jets from final state splitting of a virtual gluon into a b-quark pair (GSP) are disfavored, as this process typically produces b-jet pairs with small opening angle.

2 Event and object selection

A detailed description of the CMS detector can be found in Ref. [6]. This analysis is performed using pp and PbPb data recorded in 2015 at $\sqrt{s_{\mathrm{NN}}}$ = 5.02 TeV. The pp sample corresponds to an integrated luminosity of 25.8 pb^{-1} while the PbPb sample to an integrated luminosity of 404 μb^{-1}. The CMS online event selection employs a hardware-based level-1 trigger (L1) and a software-based high level trigger (HLT). Events were selected using single jet triggers in both pp and PbPb collisions. The jet triggers used in this analysis are fully efficient with respect to the offline leading jet selection of p_{T} >100 GeV. For PbPb collisions, b-tagging algorithms are applied at the HLT to reduce the data volume. This is achieved by performing a simplified version of the charged particle tracking and vertex reconstruction in regions of the detector defined by high p_{T} jets. The efficiency of the online b-tagging is evaluated using single jet triggers, and is in the range of 70–90% depending on collision centrality.

To reject non-collision processes such as beam-gas interactions, events are required to have at least one reconstructed primary vertex and to deposit an energy of at least 3 GeV in at least 3 towers in both forward hadron (HF) calorimeters. The HF detectors are also used to estimate the collision centrality, evaluated as a percentile of the total transverse energy.

The anti-k$_{\mathrm{T}}$ algorithm [7] is used to cluster jets from objects produced by the CMS particle-flow algorithm [8], which combines information from the various subdetector systems. In PbPb collisions, the heavy-ion background is subtracted event-by-event with an algorithm that is a variant of an iterative noise/pedestal subtraction technique [9]. The jet energy is calibrated as a function of η and p_{T} following the procedure described in Ref. [10]

The identification of b jets is achieved using the Combined Secondary Vertex (CSV) discriminator. This discriminator takes as input a number of properties of the reconstructed secondary vertex (SV), such as its flight distance, invariant mass and number of tracks. For events in which no SV is properly reconstructed, the displacement of selected tracks is used. Details of the algorithm can be found in Ref. [11]. The performance of the CSV algorithm to identify b-jet pairs is shown in Fig. 1. The efficiency and purity is evaluated in simulation as a function of the b-tagging selection variable for pp and PbPb collisions for different centrality intervals. A tight selection on the CSV discriminator is applied in this analysis, as indicated on the figure, leading to a b-dijet purity of around 90% with an efficiency in the range of about 10–35% depending on collision system and centrality.

The data are compared to simulated samples generated with PYTHIA 6.4 [12], tune Z2 [13]. To compare with PbPb data, PYTHIA events are embedded in an underlying event produced with HYDJET 1.9 [14]. Whereas the various tunes of PYTHIA used to compare to data from the LHC give a reasonable description of non-identified dijets (e.g., in Ref. [15]), they fail to adequately describe the angular and momentum correlation between b-jet pairs for the kinematic range probed by this measurement, as shown in the x_{J} (the ratio of subleading to leading jet p_{T}) and $\Delta\phi$ (the azimuthal opening angle between the leading and subleading jets) distributions in Fig. 2. In particular, PYTHIA tends to overpredict the dijet imbalance, which can be traced back to a poor modeling of the FEX contribution as previously noted by CDF [16]. While an improved modeling of this process can be achieved by softening the initial state radiation, this would have an impact on other observables, in particular the dijet p_{T} balance. Instead the contribution of the three heavy flavor production modes are reweighted according to the following procedure. Three exclusive categories of events are defined, using jets within $|\eta|$ <1.5:

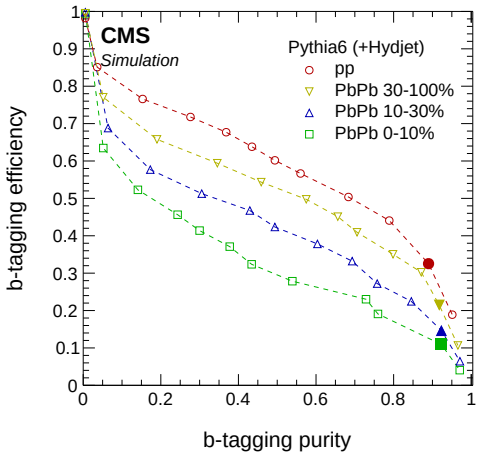

Figure 1: The b-dijet purity vs. efficiency as a function of the value of the selection on the CSV discriminator in simulation. Each marker represents a different selection on the CSV variable. Several different centrality intervals of PbPb, as well as pp collisions, are shown, as indicated in the legend. The closed symbols indicate the working point used in this analysis.

- The two highest p_{T} jets are b-tagged and back-to-back ($|\Delta\phi_{1,2}| > 2\pi/3$)
- The first and third highest p_{T} jet are b-tagged and back-to-back ($|\Delta\phi_{1,3}| > 2\pi/3$)
- The first and third highest p_{T} jet are b-tagged and nearby ($|\Delta\phi_{1,3}| < \pi/3$)

In simulation, these categories are found to be dominated by FCR, FEX, and GSP events, respectively. We reweight the contribution of each process in simulation such that the relative abundance of these three categories of events are the same as they are in data. The relative occurrence of the production processes in these categories and relative occurrence of three categories in data and MC are shown in Tables 1 and 2. Table 3 shows the relative contribution of the three production processes before and after the reweighting. The contribution of the FCR process to the selected b-dijet events is found to be at the level of 70% in PYTHIA 6 after the reweighting procedure is applied. Figure 3 shows the improved agreement of the x_{J} and $\Delta\phi$ distributions between data and simulation after reweighting.

Category	FCR	GSP	FEX
$\|\Delta\phi_{1,2}\| > 2\pi/3$	57%	17%	26%
$\|\Delta\phi_{1,3}\| > 2\pi/3$	11%	27%	62%
$\|\Delta\phi_{1,3}\| < \pi/3$	0%	83%	17%

Table 1: Relative contributions of production process in PYTHIA to jet pair categories.

Category	Data	MC
$\|\Delta\phi_{1,2}\| > 2\pi/3$	56%	46%
$\|\Delta\phi_{1,3}\| > 2\pi/3$	37%	49%
$\|\Delta\phi_{1,3}\| < \pi/3$	7%	5%

Table 2: Relative contributions of jet pair categories in pp data and PYTHIA.

Process	Default	Reweighted
FCR	53%	70%
FEX	33%	9%
GSP	14%	21%

Table 3: Contributions of the production processes in PYTHIA before and after reweighting.

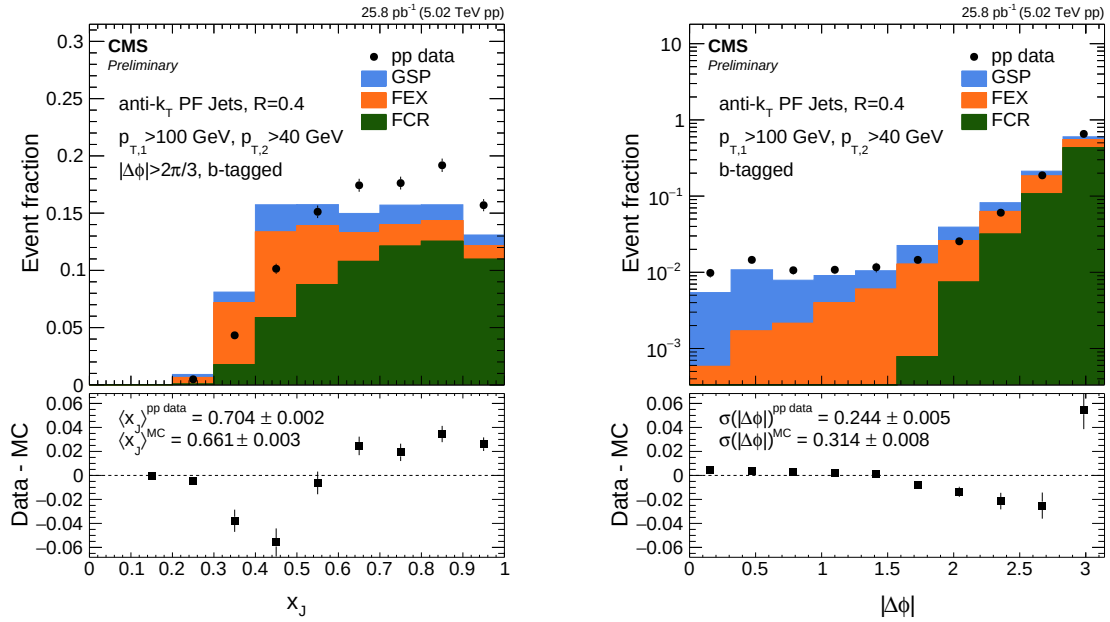

Figure 2: The distributions of x_J (left) and $\Delta\phi$ (right) in pp collisions before flavor process reweighting. Data are shown in solid points, while the stacked histograms show the contributions of different processes in PYTHIA 6.

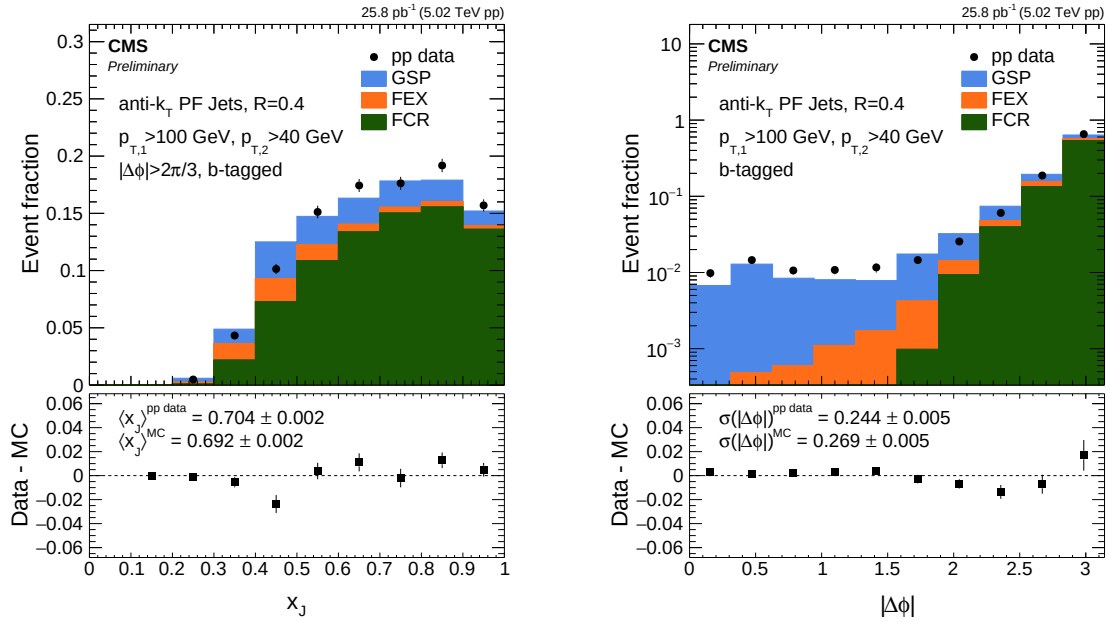

Figure 3: The distributions of x_J (left) and $\Delta\phi$ (right) in pp collisions after flavor process reweighting. Data are shown in solid points, while the stacked histograms show the contributions of different processes in PYTHIA 6.

3 Data analysis

Dijets are selected from the two highest p_T jets within a window of $|\eta| < 1.5$. The p_T of the leading and the subleading jet are required to be above 100 and 40 GeV, respectively. To select "signal" pairs, which are produced from a single hard scattering, the jets are required to be back-to-back in azimuthal opening angle with the selection of $|\Delta\phi| > 2\pi/3$. The $\Delta\phi$ distributions for central (0-10%) PbPb collisions for inclusive dijets and dijets for which both the leading and subleading jets are tagged are shown in Fig. 4. Despite this selection, the leading jet can be paired with a subleading jet that is not from the same nucleon-nucleon interaction. To subtract this contribution, we exploit the fact that such combinatorial pairs are uniform in $\Delta\phi$, and subtract the contribution of pairs from a control region where combinatorial background dominates over the signal pairs. The region is chosen to be $|\Delta\phi| < \pi/3$, which spans the same fiducial region as the back-to-back selection, and which is also symmetric with respect to elliptic flow.

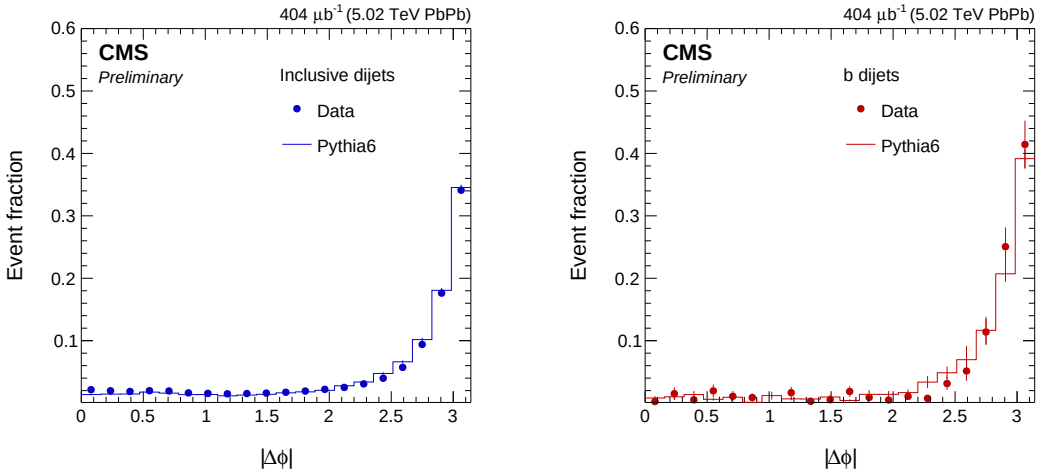

Figure 4: Distributions of the azimuthal opening angle ($\Delta\phi$) between the leading and subleading jet for central (0-10%) PbPb collisions for inclusive dijets (left) and b dijets (right).

Aside from subtracting the combinatorial component, we also also need to correct for the contribution of signal pairs that are lost when there is a combinatorial jet of higher p_T than the signal partner jet. To achieve this, an efficiency correction is derived, which is the inverse of the probability that a jet of a given p_T was found, i.e, not obscured by a combinatorial jet of larger p_T. This efficiency is again obtained from the small angle control region, by obtaining the cumulative distribution function of the p_T spectrum of the highest p_T jet in this region: $\epsilon(p_T) \equiv 1 - \frac{1}{N}\int_{p_T}^{\infty} \frac{dN}{dp_T^{max}} dp_T^{max}$. This efficiency is binned in fine bins of centrality and applied as a jet-by-jet weight factor. The corrections are shown in Fig 5. The left plot shows the corrections derived from PbPb data and from simulation. For the latter, the correction based on purely combinatorial jets is shown as well, to show the slight effect from contamination of signal jets into the sideband region. The right panel shows the full set of corrections for PbPb data, showing how the corrections evolve with centrality class.

Although the self-normalized quantities presented in this analysis do not depend on the absolute b-tagging efficiency, the relative efficiency as a function of the p_T and η must be taken into account. Corrections are derived for both the leading and subleading jet from simulation. We also correct for the variation of the tagging efficiency within the centrality selections presented in this analysis.

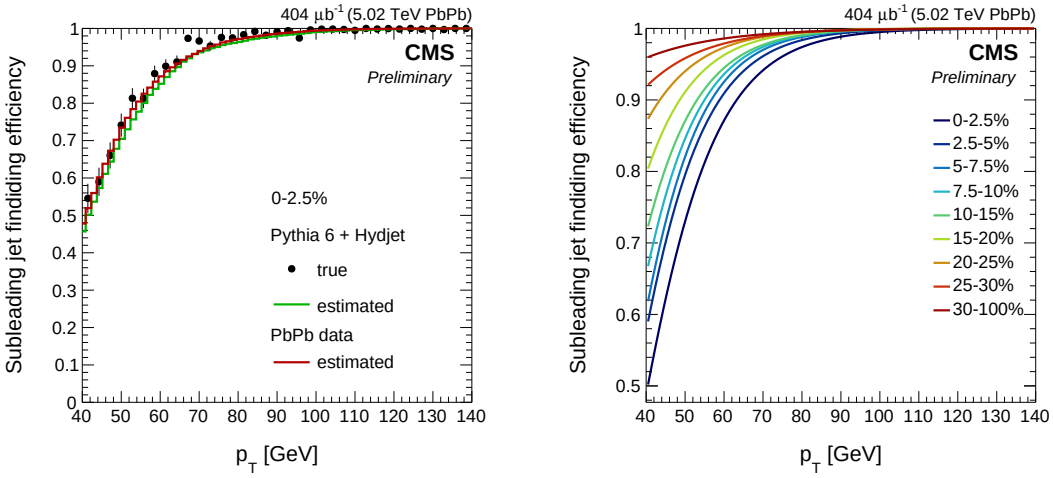

Figure 5: Left: The efficiency of finding a signal partner jet as function of its p_{T} in very central (0-2.5%) PbPb collisions, as evaluated from the small angle jet pair control region in data and simulation. In simulation, the efficiency from truth information is also shown as black points. Right: The same efficiency from PbPb data for different centrality selections.

In order to probe for quenching or other nuclear effects on the imbalance distributions, a baseline is constructed from pp data as a reference. Since the deterioration of the jet p_{T} resolution in central PbPb collisions introduces an additional effect on the x_{J} distributions, a direct comparison of PbPb and pp measurements do not immediately reflect the nuclear modifications. This issue is overcome by smearing the reconstructed jets in pp data by the amount that corresponds to the additional underlying-event fluctuations estimated in simulation, such that the pp-based reference corresponds to the same conditions as the PbPb data, leaving only the nuclear effects responsible for the differences.

4 Systematic uncertainties

The following sources of systematic uncertainty were evaluated.

- **Combinatorial jet pair subtraction** The systematic uncertainty on the combinatorial background subtraction is evaluated by varying the contribution of the sideband region. For inclusive dijets, where the sideband is composed of mostly combinatorial jets, the size of the sideband is varied by 30%, which is sufficient to cover non-closure of the procedure in simulation. For b dijets, the number of jet pairs in the sideband region is reduced by the b-tagging requirement, and is much less centrality dependent than for inclusive dijets. Embedded simulations show that the dominant contribution in the sideband region is from signal jets from gluon splitting. We therefore use the entire effect of the sideband subtraction in pp data, to estimate the systematic uncertainty on the subtraction procedure in PbPb data.
- **Subleading jet finding efficiency** The correction for the inefficiency due to losing subleading partner jets due to combinatorial jets of larger p_{T} does not perform perfectly due to several effects: a contribution of signal jets in the sideband control region ($|\Delta\phi| < \pi/3$), the finite centrality binning used and the imperfect description of the fit function employed. The systematic uncertainty associated with these corrections is evaluated from the non-closure in embedded simulation.
- **Jet energy scale** The several factors affecting the energy scale are: the overall scale uncertainty in pp [17], the difference between data and simulation, modification of jet fragmentation from quenching [3, 18–20] and effects from the underlying event subtraction. These factors are combined into two components: Correlated and uncorrelated, between the leading jet and subleading jet. The correlated component is applied to both the leading jet (by 6%) and subleading jets (by 8%) simultaneously, and has a minor impact on the x_{J} results since some part of the effect cancels in the ratio. The other component is considered to be independent, and evaluated by applying only on the subleading jets (by 2%), constituting the dominant contribution to the uncertainty.
- **Jet energy resolution**

  The resolution uncertainty in pp is determined by varying the smearing parameters that describe the jet resolution:

  $$f_{CSN}(p_T) = \sigma(p_{\mathrm{T}}^{reco}/p_{\mathrm{T}}^{gen})/ < p_{\mathrm{T}}^{reco}/p_{\mathrm{T}}^{gen} >= \sqrt{C^2 + S^2/p_{\mathrm{T}}^{Gen} + N^2/(p_{\mathrm{T}}^{Gen})^2}, \quad (1)$$

  where N is a function of centrality. To determine the uncertainty in pp, C ($\pm$0.02) and S ($\pm$0.2) are varied and particle-level jets are smeared by the corresponding amount. This variation also contains the difference of the C and S terms between pp and PbPb. For PbPb, in addition to the uncertainty in pp, the N term is varied ($\pm$2), which covers the difference in underlying event between data and MC, and the variation of the resolution within the wide centrality bins. Although the results are not unfolded for the resolution effects, the uncertainty is fully included in the data points in order to correctly evaluate any theoretical models that fold in the resolution effects for comparison.
- **Tagging efficiency (b jets only)** The tagging efficiency has a fairly flat dependence in p_{T} such that it has only a mild effect on the observed $\langle x_{\mathrm{J}} \rangle$. The size of the corrections are varied by 50% as a conservative estimate of the systematic uncertainty on this corrections. This is sufficient to cover possible differences in data and simulation observed with data-driven studies of the b-jet tagging efficiency in CMS [5, 21].

- **Mistagging (b jets only)** The effect of mistagging of non-b signal (i.e., not combinatorial) jets is evaluated by inverting the b-tagging selection for both the leading and subleading jets, both independently and simultaneously. The systematic uncertainty associated to mis-tagging is based on the imbalance of the inverted selections, taking into account the purity of the b-dijet selection in simulation, which is around 90% independent of centrality.

The absolute systematic uncertainties on $\langle x_J \rangle$ for the inclusive dijet and b dijet measurements are summarized in Tables 4 and 5, respectively.

Source	pp	30-100%	10-30%	0-10%
Combinatorial subtraction	-	0.001	0.006	0.014
Subleading jet finding	-	0.002	0.004	0.004
Energy scale	0.001	0.006	0.010	0.013
Jet resolution	0.007	0.008	0.010	0.012
total	0.007	0.010	0.016	0.023

Table 4: Absolute systematic uncertainties on $\langle x_J \rangle$ for inclusive dijets.

Source	pp	30-100%	10-30%	0-10%
Combinatorial subtraction	-	0.008	0.008	0.008
Subleading jet finding	-	0.002	0.004	0.004
Tagging efficiency	0.002	0.003	0.003	0.009
Signal mistagging	0.002	0.004	0.006	0.006
Jet energy scale	0.001	0.006	0.010	0.013
Jet resolution	0.007	0.008	0.010	0.012
total	0.008	0.014	0.018	0.023

Table 5: Absolute systematic uncertainties on $\langle x_J \rangle$ for b dijets.

5 Results

The p_T balance of inclusive and b dijets is presented, as quantified by x_J, the ratio of the subleading to leading jet p_T. Results are presented for a leading and subleading jet p_T of 100 and 40 GeV, respectively, selected from jets in $|\eta| < 1.5$. The x_J distributions for inclusive dijets and b dijets are shown for pp collisions in Fig. 6. The data are compared with simulations performed with PYTHIA 6. Figures 7, 8 and 9 show the x_J distributions for PbPb collisions with centrality selections of 30-100%, 10-30% and 0-10%, respectively. Here the data are compared to the reference obtained from pp data by smearing the p_T of each jet according to a parametrization of the resolution for the given centrality class. Figure 10 shows the mean x_J values from these distributions. The data are plotted as a function of the number of participants estimated from a Monte Carlo Glauber model [22, 23]. The number of participants is weighted by the number of collisions to account for the hard scattering bias within each bin. Both the inclusive dijet and b dijet data show a tendency towards increasing imbalance with increasing centrality. While the reference also becomes more imbalanced due to resolution effects, the magnitude of the effect is much smaller. The effect is understood to be due to jet quenching, as observed in previous inclusive dijet results [2, 15]. Within the current uncertainties, no significant difference is observed between the quenching of inclusive and b dijets. Whereas the inclusive dijets contain a mix of quark and gluon jets, the b dijets mostly originate from primary b quarks. The measurement places constraints on the possible mass and flavor dependence of quenching for the kinematic regime currently probed.

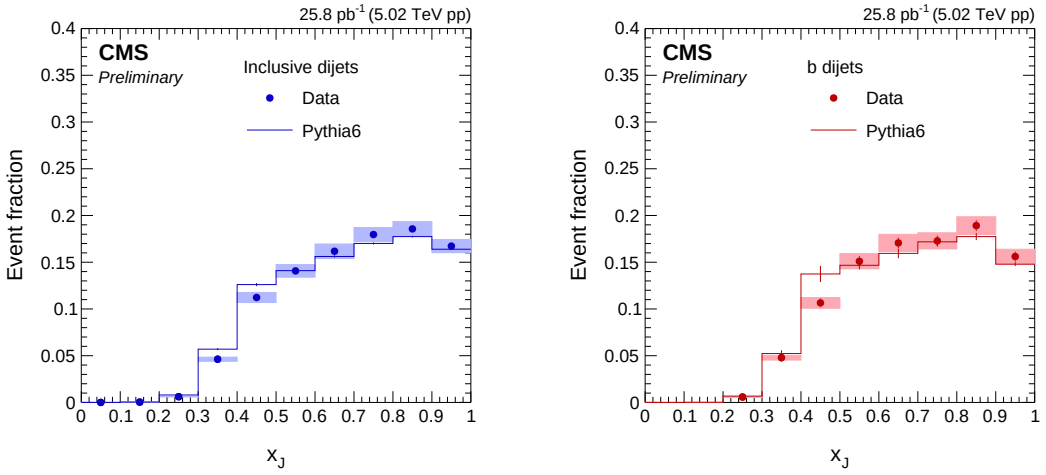

Figure 6: Distribution of x_J in pp collisions for inclusive dijets (left) and b-dijets (right). Systematic uncertainties are shown as shaded boxes, while statistical uncertainties are shown as verticial lines.

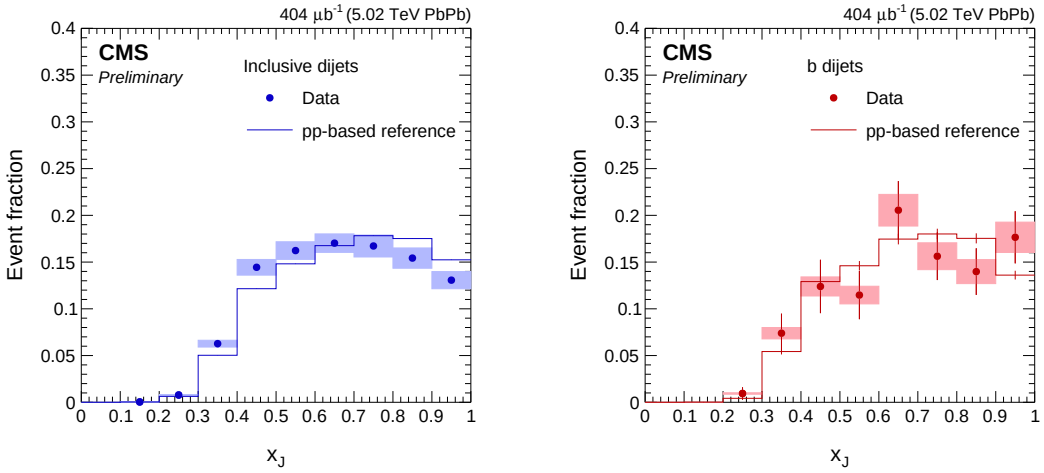

Figure 7: Distribution of x_J in peripheral (30-100%) PbPb collisions for inclusive dijets (left) and b-dijets (right). Systematic uncertainties are shown as shaded boxes, while statistical uncertainties are shown as verticial lines.

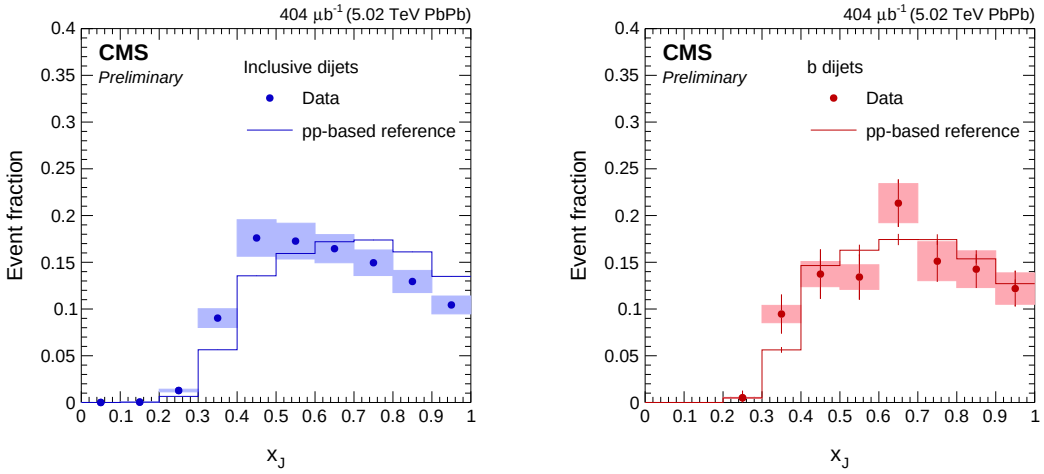

Figure 8: Distribution of x_J in mid-central (10-30%) PbPb collisions for inclusive dijets (left) and b-dijets (right). Systematic uncertainties are shown as shaded boxes, while statistical uncertainties are shown as verticial lines.

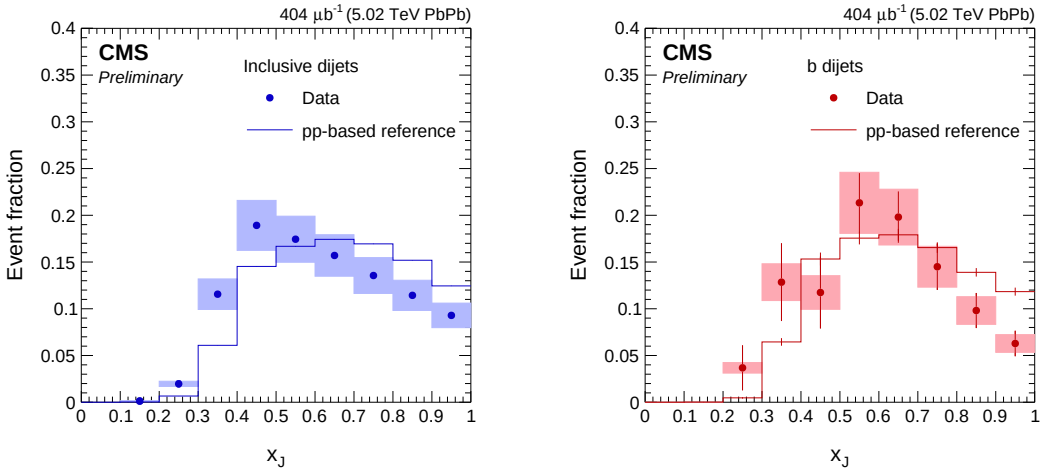

Figure 9: Distribution of x_J in central (0-10%) PbPb collisions for inclusive dijets (left) and b-dijets (right).

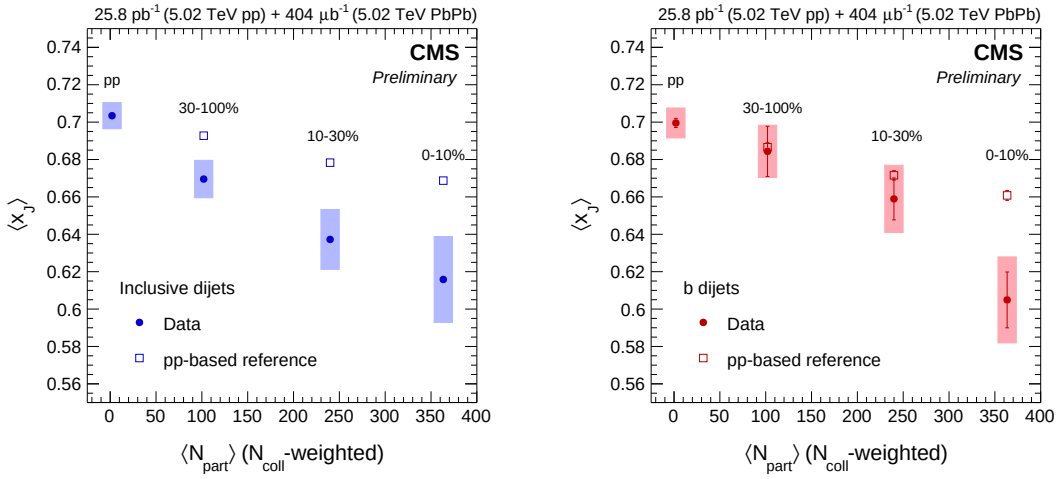

Figure 10: Mean x_J for inclusive (left) dijets and b dijets (right) in pp collisions and for different centrality selections of PbPb collisions. Systematic uncertainties are shown as shaded boxes, while statistical uncertainties are shown as verticial lines.

References

[1] ATLAS Collaboration, "Observation of a Centrality-Dependent Dijet Asymmetry in Lead-Lead Collisions at $\sqrt{s_{NN}} = 2.77$ TeV with the ATLAS Detector at the LHC", *Phys. Rev. Lett.* **105** (2010) 252303, doi:10.1103/PhysRevLett.105.252303, arXiv:1011.6182.

[2] CMS Collaboration, "Observation and studies of jet quenching in PbPb collisions at nucleon-nucleon center-of-mass energy = 2.76 TeV", *Phys. Rev. C* **84** (2011) 024906, doi:10.1103/PhysRevC.84.024906, arXiv:1102.1957.

[3] CMS Collaboration, "Measurement of transverse momentum relative to dijet systems in PbPb and pp collisions at $\sqrt{s_{\mathrm{NN}}} = 2.76$ TeV", *JHEP* **01** (2016) 006, doi:10.1007/JHEP01(2016)006, arXiv:1509.09029.

[4] Y. L. Dokshitzer and D. E. Kharzeev, "Heavy quark colorimetry of QCD matter", *Phys. Lett. B* **519** (2001) 199–206, doi:10.1016/S0370-2693(01)01130-3, arXiv:hep-ph/0106202.

[5] CMS Collaboration, "Evidence of b-Jet Quenching in PbPb Collisions at $\sqrt{s_{NN}} = 2.76$TeV", *Phys. Rev. Lett.* **113** (2014) 132301, doi:10.1103/PhysRevLett.115.029903, 10.1103/PhysRevLett.113.132301, arXiv:1312.4198. [Erratum: Phys. Rev. Lett.115,no.2,029903(2015)].

[6] CMS Collaboration, "The CMS experiment at the CERN LHC", *JINST* **3** (2008) S08004, doi:10.1088/1748-0221/3/08/S08004.

[7] M. Cacciari, G. P. Salam, and G. Soyez, "The anti-k_t jet clustering algorithm", *JHEP* **04** (2008) 063, doi:10.1088/1126-6708/2008/04/063, arXiv:0802.1189.

[8] CMS Collaboration, "Particle-flow event reconstruction in CMS and performance for jets, taus, and $E_{\mathrm{T}}^{\mathrm{miss}}$", CMS Physics Analysis Summary CMS-PAS-PFT-09-001, CERN, 2009.

[9] O. Kodolova, I. Vardanian, A. Nikitenko, and A. Oulianov, "The performance of the jet identification and reconstruction in heavy ions collisions with CMS detector", *Eur. Phys. J. C* **50** (2007) 117, doi:10.1140/epjc/s10052-007-0223-9.

[10] CMS Collaboration, "Determination of Jet Energy Calibration and Transverse Momentum Resolution in CMS", *JINST* **6** (2011) P11002, doi:10.1088/1748-0221/6/11/P11002, arXiv:1107.4277.

[11] CMS Collaboration, "Identification of b-quark jets with the CMS experiment", *JINST* **8** (2013) P04013, doi:10.1088/1748-0221/8/04/P04013, arXiv:1211.4462.

[12] T. Sjöstrand, S. Mrenna, and P. Skands, "PYTHIA 6.4 physics and manual", *JHEP* **05** (2006) 026, doi:10.1088/1126-6708/2006/05/026, arXiv:hep-ph/0603175.

[13] R. Field, "Min-Bias and the Underlying Event at the LHC", *Acta Phys. Polon. B* **42** (2011) 2631, doi:10.5506/APhysPolB.42.2631, arXiv:1110.5530.

[14] I. P. Lokhtin and A. M. Snigirev, "A Model of jet quenching in ultrarelativistic heavy ion collisions and high-p_{T} hadron spectra at RHIC", *Eur. Phys. J. C* **45** (2006) 211, doi:10.1140/epjc/s2005-02426-3, arXiv:hep-ph/0506189.

[15] CMS Collaboration, "Jet momentum dependence of jet quenching in PbPb collisions at $\sqrt{s_{NN}} = 2.76$ TeV", *Phys. Lett. B* **712** (2012) 176, doi:10.1016/j.physletb.2012.04.058, arXiv:1202.5022.

[16] CDF Collaboration, "Measurements of $b\bar{b}$ azimuthal production correlations in $p\bar{p}$ collisions at $\sqrt{s} = 1.8$ TeV", *Phys. Rev. D* **71** (2005) 092001, doi:10.1103/PhysRevD.71.092001, arXiv:hep-ex/0412006.

[17] CMS Collaboration, "CMS JEC Run I legacy performance plots", CMS Detector Performance Note CMS-DP-2015-044, CERN, 2015.

[18] CMS Collaboration, "Measurement of jet fragmentation into charged particles in pp and PbPb collisions at $\sqrt{s_{NN}} = 2.76$ TeV", *JHEP* **10** (2012) 087, doi:10.1007/JHEP10(2012)087, arXiv:1205.5872.

[19] CMS Collaboration, "Measurement of jet fragmentation in PbPb and pp collisions at $\sqrt{s_{NN}} = 2.76$ TeV", *Phys. Rev. C* **90** (2014) 024908, doi:10.1103/PhysRevC.90.024908, arXiv:1406.0932.

[20] CMS Collaboration, "Correlations between jets and charged particles in PbPb and pp collisions at $\sqrt{s_{\mathrm{NN}}} = 2.76$ TeV", *JHEP* **02** (2016) 156, doi:10.1007/JHEP02(2016)156, arXiv:1601.00079.

[21] CMS Collaboration, "Identification of b quark jets at the CMS Experiment in the LHC Run 2", CMS Physics Analysis Summary CMS-PAS-BTV-15-001, CERN, 2016.

[22] M. L. Miller, K. Reygers, S. J. Sanders, and P. Steinberg, "Glauber modeling in high energy nuclear collisions", *Ann. Rev. Nucl. Part. Sci.* **57** (2007) 205, doi:10.1146/annurev.nucl.57.090506.123020, arXiv:nucl-ex/0701025.

[23] B. Alver et al., "Importance of correlations and fluctuations on the initial source eccentricity in high-energy nucleus-nucleus collisions", *Phys. Rev. C* **77** (2008) 014906, doi:10.1103/PhysRevC.77.014906, arXiv:0711.3724.